Revista Brasileira de Física, Vol. 17, no 3, 1987

A Prospective View of Instability Control in Pinches and Tokamaks by Plasma Current Shaping

A. TOMIMURA
Instituto de Física, Universidade Federal Fluminense, 24210, Niterói, RJ, Brasil

Recebido em 14 de novembro de 1986

Abstract A computing code based onan implicitdifference scheme has been employed to solve the set of partial differential equations (radial and time dependent) for the perturbed variables which describethe resistive magnetohydrodynamic (MHD) instability in pinches and tokamaks in order to assess the conditions for the appearance of stability windows insome of the input parameters used. It is shown that it is possibletoinhibit or even suppress the m=2, n=l and m=3, n=2 tearing modes by shaping the longitudinal plasma current density in the form of a small, localized distortion on a previously chosen smooth profile for the equilibrium configuration. The corresponding windows appear in the ínput parameter space q_a, the safety factor at the current channel position, for a fixed position of the distortion as well as in the parameter space RR,, the radial position of the distortion, for a fixed q_a; in both cases, the distortion is localized near and inside the singular surface.

1. INTRODUCTION

The method of instability control in tokamaks by plasma current shaping has its main practical relevance in providing ways of delaying or even suppressing the appearance of the most dangerous instability in tokamak discharges known by the generic name of disruptive instability[1], characterized in its initial phase by a slowly growing magnetic perturbation and terminating with a sudden loss of confinement with the plasma current dropping very rapidly to zero (e.g., 20 ms in JET). Such an instability has long been suspected of being caused by the resistive magnetohydrodynamic (MHD) tearing modes.

The method is based upon the fact that the growth of tearing modes depends on the existence of a current density gradient along the plasma radius so that if this gradient is locally reduced somewhere inside the current channel, the growth of a given mode can be reduced or even suppressed. Toi et al[2] give evidence that the resulting distribution of current can be obtained experimentally and one of the promis-

sing proposals is to locally control the temperature profile either by electron cyclotron resonance heating or through localized current drive?

In this work we adopt the procedure established by Robinson, D. C., et al[4], which differs from that of Glasser et al[5] who obtained a tearing mode stable distribution of current density by minimizing A' for each mode and for different values of q. Our investigation has been limited to the analysis of the conditions for the control of the $m=2$, $n=1$ and $m=3$, $n=2$ tearing modes in diffuse pinches and (straight) tokamaks, as these are the most probable candidates to explain the disruptive nature of the instability.

For the equilibrium configuration we have employed the Culham Model[4] because of its large current gradient near the edge of the current channel and therefore strongly unstable relative to tearing modes. A gaussian with a small width and amplitude is then superimposed on the poloidal field distribution, distorting it locally with a similar effect on the current density profile (through Ampère's law). This new equilibrium configuration in then established through some of the free parameters of the input data of an existing, linear, one dimensional, resistive MHD instability code, which solves the set of partial differential equations for the perturbed variables. We then look at the effect that the small distortion on the current density profile has onthe growth rate of a particular mode by either varying the input values of q_a or the values of the radial position of the distortion. In both cases, windows of stability have been found which reveal that tearing mode stable configurations can be achieved by this method.

2. (a) – BASIC EQUATIONS AND ASSUMPTIONS

In this work, the plasma is described by the MHD equations for a single fluid, viz., the continuity equation,

$$\frac{\partial \rho}{\partial t} + \nabla . (\rho \vec{V}) = 0 \quad , \tag{1}$$

the equation of motion

$$\rho \left(\frac{\partial \vec{V}}{\partial t} + \vec{V} . \nabla \vec{V} \right) = \frac{\vec{J} \times \vec{B}}{c} - \nabla p \quad , \tag{2}$$

Ohm's law,

$$E + \vec{V}\times\vec{B}/c = \eta\vec{J} \quad , \tag{3}$$

and by Maxwell's equations and Ohm's law combined in the single equation

$$\frac{\partial\vec{B}}{\partial t} = \nabla\times(\vec{V}\times\vec{B}) - \left(\frac{c^2}{4\pi}\right)\nabla\times(\eta\nabla\times\vec{B}) \quad , \tag{4}$$

where p, $\vec{V}$, p, $\vec{J}$, $\vec{B}$, $\vec{E}$ and η the density, flow velocity, scalar pressure, current density, magnetic and electric fields and resistivity respectively.

Denoting by the subscripts (0) and (1) the equilibrium and perturbed quantities respectively, one gets, assuming a zero flow velocity $\vec{V}_0$, the zeroth order equations

$$(\nabla\times\vec{B}_0)\times\vec{B}_0 - \nabla p_0 = 0 \quad , \tag{5}$$

$$\nabla\times(\eta_0\nabla\times\vec{B}_0) = 0 \quad , \tag{6}$$

and the linearized equations for the first order variables

$$\rho_0\frac{\partial\vec{V}_1}{\partial t} = \frac{1}{4\pi}\left[(\vec{B}_0.\nabla)\vec{B}_1 - (\vec{B}_1.\nabla)\vec{B}_0 - \nabla(\vec{B}_0.\vec{B}_1)\right] - \nabla p_1 \quad , \tag{7}$$

$$\frac{\partial\vec{B}_1}{\partial t} = \nabla\times(\vec{V}_1\times\vec{B}_0) - \left(\frac{c^2}{4\pi}\right)\nabla\times(\eta_0\nabla\times\vec{B}_1) \quad , \tag{8}$$

where we have assumed and unperturbed resistivity and constant pressure throughout the plasma in order to avoid rippling and interchange modes. The plasma is also considered incompressible, i.e., $\nabla.\vec{V}_1 = 0$ with a constant density $p = \rho_0$ along the plasma radius, which extends up to a conducting wall.

The sic equations implicit in eqs.(7) and (8) for the components of $\vec{V}_1$ and $\vec{B}_1$ can be further reduced if one takes the curl of eq. (7) in order to eliminate the perturbed pressure p_1 and then using $\nabla\cdot\vec{V}_1 = \nabla\cdot\vec{B}_1 = 0$ to eliminate V_{1z} and B_{1z} from the resulting set of equations. Now, by considering only perturbations of the form $f_1(r,t)\exp(im\theta+ik_z z)$,

these equations reduce to

$$\frac{\partial B_{r1}}{\partial t} = iFV_{r1} + \frac{c^2\eta_0}{4\pi}\left[\frac{\partial}{\partial r}\left(\frac{1}{r}\frac{\partial rB_{r1}}{\partial r}\right) - hB_{r1} - \frac{2im}{r^2}B_{\Theta 1}\right], \tag{9}$$

$$\frac{\partial B_{\Theta 1}}{\partial t} = iFV_{\Theta 1} - \left[r\frac{\partial}{\partial r}\left(\frac{B_{\Theta 0}}{r}\right)\right]V_{r1} + \frac{c^2\eta_0}{4\pi}\left[\frac{\partial}{\partial r}\left(\frac{1}{r}\frac{\partial rB_{\Theta 1}}{\partial r}\right) - hB_{\Theta 1} + \frac{2im}{r^2}B_{r1}\right]$$

$$+ \frac{c^2}{4\pi}\frac{\partial \eta_0}{\partial r}\left(\frac{1}{r}\frac{\partial rB_{\Theta}}{\partial r} - \frac{im}{r}B_{r1}\right), \tag{10}$$

$$-4\pi\rho_0 i\frac{\partial}{\partial t}\left[\frac{\partial}{\partial r}\left(\frac{1}{r}\frac{\partial rV_{r1}}{\partial r}\right) - hV_{r1} - \frac{2im}{r^2}V_{\Theta 1}\right] =$$

$$= F\left[\frac{\partial}{\partial r}\left(\frac{1}{r}\frac{\partial rB_{r1}}{\partial r}\right) - hB_{r1} - \frac{2im}{r^2}B_{\Theta 1}\right] + \left[-\frac{m}{r^2}\frac{\partial}{\partial r}\left(r\frac{\partial B_{\Theta 0}}{\partial r}\right) - \frac{m}{r^3}B_{\Theta 0}\right.$$

$$\left. - k_z r\frac{\partial}{\partial r}\left(\frac{1}{r}\frac{\partial B_{z0}}{\partial r}\right)\right]B_{r1} + \left[-\frac{2m}{r^2}B_{\Theta 0}\right]\frac{\partial B_{r1}}{\partial r} + \left[-\frac{2h}{r}B_{\Theta 0}\right]iB_{\Theta 1}, \tag{11}$$

$$-4\pi\rho_0\frac{\partial}{\partial t}\left[\frac{\partial}{\partial r}\left(\frac{1}{r}\frac{\partial rV_{\Theta 1}}{\partial r}\right) - hV_{\Theta 1} + \frac{2im}{r^2}V_{r1}\right]$$

$$= -iF\left[\frac{\partial}{\partial r}\left(\frac{1}{r}\frac{\partial rB_{\Theta 1}}{\partial r}\right) - hB_{\Theta 1} + \frac{2im}{r^2}B_{r1}\right]$$

$$- \left[\frac{1}{r}\frac{\partial}{\partial r}(rB_{\Theta 0})\right]\left[\frac{\partial}{\partial r}\left(\frac{1}{r}\frac{\partial rB_{r1}}{\partial r}\right) - hB_{r1}\right]$$

$$- \left[\frac{1}{r^2}\frac{\partial}{\partial r}\left(r^2\frac{\partial^2 B_{\Theta 0}}{\partial r^2}\right) + \left(\frac{2m^2-1}{r^2}\right)\frac{\partial B_{\Theta 0}}{\partial r} + \frac{B_{\Theta 0}}{r^3} + \frac{2mk_z}{r}\frac{\partial B_{z0}}{\partial r}\right]B_{r1}$$

$$- \left[2\frac{\partial}{\partial r}\left(\frac{1}{r}\frac{\partial rB_{\Theta 0}}{\partial r}\right)\right]\frac{\partial B_{r1}}{\partial r} - \left[2\left(\frac{m}{r}\frac{\partial B_{\Theta 0}}{\partial r} + k_z\frac{\partial B_{z0}}{\partial r}\right)\right]i\frac{\partial B_{\Theta 1}}{\partial r}$$

$$+ \left[-\frac{m}{r^2}\frac{\partial}{\partial r}\left(r\frac{\partial B_{\Theta 0}}{\partial r}\right) + \frac{3m}{r^3}B_{\Theta 0} - \frac{k_z}{r}\frac{\partial}{\partial r}\left(r\frac{\partial B_{z0}}{\partial r}\right)\right]iB_{\Theta 1}, \tag{12}$$

where $F = mB_{\Theta 0}(r)/r + k_z B_{z0}(r)$ and $h = m^2/r^2 + k_z^2$.

For numerical computation these equations were conveniently written in terms of the normalized independent variables for radial pos-

ition and time, $x = r/a$ and $\tau = t/\tau_R$ respectively, and the following dimensionless dependent variables,

$$\psi = B_{r1}/B \quad , \quad \phi = iB_{\theta 1}/B \quad , \quad W = -ik\tau_R v_{r1} \quad , \quad U = k\tau_R v_{\theta 1} \quad , \tag{13}$$

where a is the current channel radius, τ_R the resistive diffusion time, $k = (m^2/R_s^2 + k_z)^{1/2}$ with R_s standing for the radial position of the singular surface and B is the characteristic value of the magnetic field.

The boundary conditions suitable to resistive $m \geq 2$ modes which are of' interest in this work are

$$B_{r1} = B_{\theta 1} = V_{r1} = V_{\theta 1} = 0 \quad \text{at} \quad r = 0 \tag{14}$$

$$B_{r1} = V_{r1} = 0 \quad \text{at} \quad r = R_W \text{ (the conducting wall)} \tag{15}$$

$$B_{\theta 1} = \frac{imR_W}{m^2 + k_z^2 R_W^2} \left. \frac{\partial B_{r1}}{\partial r} \right|_{r=R_W} \tag{16}$$

$$V_{\theta 1} = \frac{imR_W}{m^2 + k_z^2 R_W^2} \left. \frac{\partial V_{r1}}{\partial r} \right|_{r=R_W} \tag{17}$$

provided $\vec{k}.\vec{B} \neq 0$ at the wall and the pressure $p \rightarrow 0$ as $r \rightarrow R_W$.

In addition to the boundary conditions given, an initial perturbation has to be specified for one of the variables, say V_0 in order to begin the calculation. A specific form has been chosen for $V_{r1}(r,0)$ but the results with other forms have shown to be quite independent of the initial perturbation (as it should be).

The set of equations (9)-(12), together with the boundary conditions (14)-(17) can be seen elsewhere[4,6,7] in their more general forms, where the equilibrium resistivity and pressure profiles, heatconduction and viscosity effects are included. In particular, the boundary conditions are fully discussed in reference 4.

Finally, as one can see by inspection of equations (9)-(17), the

calculation of the perturbed quantities requires the knowledge of the equilibrium profiles of $B_{\Theta_0}(r)$ and $B_{z_0}(r)$ which, in their turn, can be either given as numerical data directly taken from some experiments or by modelling the equilibrium by specifying the profiles of some relevant parameter (usually functions based on experimental data) and constructing the whole equilibrium functions from it. A number of equilibrium models have been constructed in the past by various authors[8,9,10] to study resistive instabilities and amongst them we chose the one which bestsuits our studies, viz., the Culham Model. In it, the axial current density whose form is based on the measured temperature profile on the T3-A tokamak, is given by

$$J_{z_0} = \begin{cases} J_0 \left[1 - (r/a)^M\right]^N & r \leq a \\ 0 & r \geq a \end{cases} \tag{18}$$

where N and M are usually taken to be 2 and 4 respectively, a isthe current channel radius and J_0 is a normalization factor.

From J_{z_0} given by eq. (18), we get B_{Θ_0} by integrating the z-component of Ampère's law,

$$\frac{1}{r}\frac{\partial (rB_{\Theta_0})}{\partial r} = \frac{4\pi}{c} J_{z_0} \quad , \tag{19}$$

and using B_{Θ_0} so obtained and J_{z_0}, we combine the (force-free) pressure balance

$$J_{z_0} B_{\Theta_0} = J_{\Theta_0} B_{z_0} \quad , \tag{20}$$

with the Θ-component of Ampère's law,

$$\frac{\partial B_{z_0}}{\partial r} = -\frac{4\pi}{c} J_{\Theta_0} \quad , \tag{21}$$

to get

$$\frac{\partial B^2_{z_0}}{\partial r} = -2 \left(\frac{4\pi}{c}\right) J_{z_0} B_{\Theta_0} \quad , \tag{22}$$

which, by integration, gives $B_{z_0}(r)$

Now, by choosing the characteristic value of the normalization factor B_0 for the magnetic fields $B_{\Theta 0}$ and B_{z0} to be

$$B_0 = \frac{4\pi}{c} J_0 \, a \quad , \tag{23}$$

the normalized forms of J_{z0}, $B_{\Theta 0}$, B_{z0} and $J_{\Theta 0}$ read

$$\tilde{J}_z(x) = \begin{cases} (1-x^M)^N & , \quad x \leq 1 \\ 0 & , \quad x \geq 1 \end{cases} \tag{24}$$

$$\tilde{B}_\Theta(x) = \begin{cases} N! \sum_{K=0}^{N} \dfrac{(-)^K x^{KM+1}}{(N-K)!K!(KM+2)} & , \quad x \leq 1 \\ \tilde{B}_\Theta(1)/x & , \quad x \geq 1 \end{cases} \tag{25}$$

$$\tilde{B}_z(x) = \begin{cases} \tilde{B}_z^2(1) + 2(N!)^2 \sum_{L=0}^{N} \sum_{K=0}^{N} \dfrac{(-)^{L+K}\left[1 - x^{(L+K)M+2}\right]}{(N-L)!L!(N-K)!K!(KM+2)\left[(K+L)M+2\right]} & x \leq 1 \\ \tilde{B}_z^2(1) & , \quad x \geq 1 \end{cases} \tag{26}$$

$$\tilde{J}_\Theta(x) = \tilde{J}_z(x)\ \tilde{B}_\Theta(x)/\tilde{B}_z(x) \quad , \tag{27}$$

where $x = r/a$ is the normalized radius. These expressions still leave $B_z(1)$ undetermined, which could be used as a free parameter. We use instead the value of the safety factor $q_a = rB_z(r)/R_0\, B_\Theta(r)$ at $r = a$, that is,

$$q_a \equiv q(1) = \frac{\tilde{B}_z(1)}{\tilde{R}_0 \tilde{B}_\Theta(1)} \quad , \tag{28}$$

where $\tilde{R}_0$ is the normalized (to a) major radius of the torus.

Therefore, given N, M, q_a and $\tilde{R}_0$, the equilibrium profiles of

$\tilde{J}_z$, $\tilde{B}_0$, $\tilde{B}$ and $\tilde{J}$ are defined, as well as the (normalized) function $\tilde{F}$ given by

$$\tilde{F} = \frac{1}{\alpha} \left(\frac{m}{x} \nu\Theta + Kz\tilde{B}z \right) \quad , \tag{29}$$

where $o = (m^2/x_s^2 + K_z^2)^{1/2}$, x_s being the normalired radial position of the singular surface and $K_z = k_z\, a$.

2. (b) – COMPUTATIONAL PROCEWRE

In order to solve the set of eqs. (9)-(12) with the boundary conditions given by eqs. (14)-(17) and the equilibrium model described before, we have used an existing code[a] which treats them as an initial boundary value problem and uses an implicit finite-difference scheme where the four (normalized) equations for B_{r1}, $B_{\Theta 1}$, V_{r1} and $V_{\Theta 1}$ are solved simultaneously at integral time steps using a single vector difference equation (see details in refs. 6 and 8). Given the input data and the initial perturbation, the code then computes the solution ofthe equations and evaluates the growth of the perturbation at each time step using $P = (\partial\psi(r,t)/\partial t)/\psi$, where ψ can be any of the four relevant parameters (we have chosen B_{r1} and $V_{\Theta 1}$); after a number of time steps the unstable mode is found when P settles down to a positive constant indicating an exponential growth.

To run the code, it is necessary to specify the equilibrium profiles for $\tilde{B}_O$ and $\tilde{B}_z$ as well the quantities $\rho_0/\langle\rho\rangle$ and $\eta_0/\langle\eta\rangle$, · where the brackets stand for characteristic values. The first two are given by the equilibrium model (the Culham Model) built in rhe code as a sub-routine and the third one is assigned the value unit, meaning that the (constant) value of ρ_0 is identical to its characteristic value. In addition, we must also specify the values of $\tilde{R}_0$, m, k_z $(=-\eta/\tilde{R}_0)$ and the magnetic Reynolds number S, defined as the ratio between the resistive diffusion time and the Alfven transit time, $\tau_R = 4\pi L^2/c^2\langle\eta\rangle$ and $\tau_H = L(4\pi\langle\rho\rangle)^{1/2}/B$ respectively, that is

$$S = \tau_R/\tau_H \quad , \tag{30}$$

(a) at Culham Laboratory, named RIPPLE4A - see also ref.6.

where L is a characteristic length (which in our case, we identified it with the current channel radius a) and B is a characteristic value for the magnetic field.

Now, the normalized growth rate P is related to the original growth rate γ by the relation $P = \tau_R \gamma$, so that one can also write

$$P = S(\gamma \tau_H) \quad . \tag{31}$$

This formula provides a straightfoiward conversion from P to γ and vice-versa whenever comparisons with analytical results are needed. For example, Shafranov's free-boundary problem[11] has the growth of kink modes given by

$$\gamma^2 = \frac{B_{\theta a}^2}{2\pi\rho a^2} (m - nq_a) \left\{ 1 - \frac{m - nq_a}{1-(a/b)^{2m}} \right\} \quad , \tag{32}$$

in the interval $m - 1 + (a/b)^{2m} \leq q_a < m$ with a maximum growth given by

$$\gamma_{max}^2 = \frac{B_{\theta a}^2}{8\pi\rho a^2} \left[1 - (a/b)^{2m} \right] \quad , \tag{33a}$$

where a is the plasma radius (= current channel radius) and b is the conducting wall radius. Choosing for convenience, $B = 2B_{\theta a}$ and $\langle\rho\rangle = \rho$ (constant)[(b)] then

$$P_{max} = S\tau_H \gamma_{max} = \frac{S}{2\sqrt{2}} \left[1 - (a/b)^{2m} \right]^{1/2} \tag{33b}$$

where one can see that the growth rate of the ideal kink mode varies linearly with S.

3. NUMERICAL RESULTS

(a). Numerical results for the standard Culham Model

We begin this section by exhibiting a series of results from the usual Culham Model in order to set up a standard upon which one can make

(b) To comply with the normalization factors chosen in the code.

comparisons and draw some conclusions from results presented by a modified Culham Model in part (b). We also take this opportunity to recall some of the characteristics of the unstable modes presented by the standard model.

In order to study the variation of the growth rates of the resistive modes as a function of the safety factor q_a, a number of cases with the same entry data but q_a have been computed. Fig. 1 shows the normalized growth rate and the normalized singular surface radius x_s (for which $\vec{k}.\vec{B}(r_s)=0$), plotted against q_a, of the unstable modes m=2, n=1 and m=3, n=2 found with the values of q_a taken from the intervai $0 \leq q_a \leq 4.5$. The relevant entry data were as follows: k_z = -0.25, S = = 1000, $\tilde{R}_W = R_W/a$ = 1.4, $\tilde{R}$ = 4., (N,M) = (2,4) (see eq. (24) for the current profile), JMAX = 301 (the No. of mesh points), NMAX = 300 (the No. of time steps), for the m=2, n=1 modes and the same data as before for the m=3, n=2 modes, except k_z = -0.50.

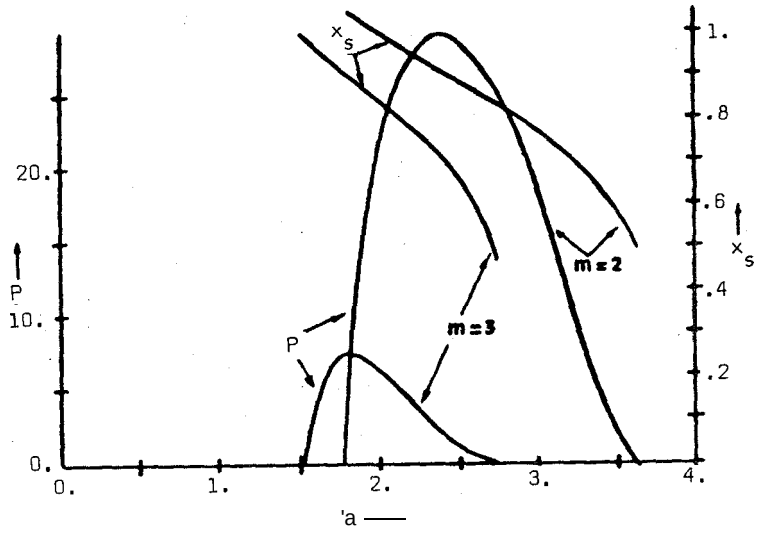

Fig.1 - The normalized growth rate P and the singular surface radius x_s as a function of q_a, for the m=2, n=1 and m=3, n=2 tearing modes.

The normalized resistivity $\tilde{\eta} = \eta/\langle\eta\rangle$ has been made constant (=1.) throughout the plasma radius and will remain so unless otherwise stated.

The plots in fig. 1 reveal, for the particular set of parameters above, that (i) for both modes, the singular surface radii x_s are well below the plasma radius $\tilde{R}_W$ (=1.5) and therefore the restriction imposed on the boundary conditions is being fulfilled (i.e., $\vec{k}.\vec{B} \neq 0$ at $r=R_W$). In addition, most of the unstable modes have been found with the singular surfaces inside the current channel radius (x=1); (ii) the maximum growth rates attainable are 28.97 at q_a = 2.4 for the m=2, n=1 mode and 7.36 at q_a = 1.8 for the m=3, n=2 mode, the former existing in the interval $1.77 \leq q_a \leq 3.60$ and the latter appearing in the interval $1.514 \leq q_a \leq 2.70$; (iii) the overlapping of these intervals, viz., $1.77 \leq q_a \leq 2.70$ indicates the region of q_a where both modes occur with their respective maximum growth; (iv) the region on the parameter space q_a for the existence of the m=2 mode is about twice larger than the m=3 mode, with a growth rate for the maximum about four times bigger.

The results above comply with existing analytical theory on the relative values of growth rates for ideal and resistive modes[12], viz., $1 << P_{max}$ (resistive) $<< P_{max}$(ideal), where P_{max} stands for the maximum normalized growth rate, the lower limit (=1) stands for the rate of field diffusion and the upper one is the rate at which the ideal kink mode grows in an infinite conductivity plasma. As compared to the results of Shafranov's step model[11] where the kink modes have a maximum growth of P_{max} = 304.07 (from formula 33b), existing in the interval $1.26 \leq q_a \leq 2$, one can see that the growth rates of tearing modes (the tearing character will be shown next) represented in fig. 1 show a much lower value (~ 10 times smaller) and a wider interval of q_a for their existence.

'The next series of figures show plots for a typical case run by the code with q_a chosen from the curve m=2 in fig. 1, viz., q_a = 2.4. Fig.2(a) shows the equilibria profiles yielded by the Culham Model for this value of q_a (and therefore a fixed value of $\tilde{B}_{z_0}(1)$ according to eq. (28)). These graphs exhibit the radial profiles for the normalized $\tilde{J}_z$, $\tilde{B}_z$, $\tilde{B}_\Theta$, the safety factor $q = rB_z(r)/R_0B_O(r) = x\tilde{B}_z(x)/\tilde{R}_0\tilde{B}_\Theta(x)$ and the

function $\tilde{F}$ given by formula (29). The point where $\tilde{F}$ crosses the axis define the (normalized) position x_s of the singular surface. We note that there would have been no rernarkable differences in the functional forms of the various parameters if we had chosen any other value of the input parameter q_a, apart from $\tilde{F}$ which would cross the axis at points x_s (listed as the value of R_s at the bottom of fig.2(a)) in decreasing succession corresponding to an increasing succession of q_a values.

Fig.2(b) illustrates how the correct modes are picked up by the code in a random fashion until the growth rates settle down to a positive value. The plots of $P(t) = (\partial\psi/\partial x)/\psi$, where ψ has been set to both B_{r1} and $V_{\Theta 1}$, are labelled $P(B_r)$ and $P(V_t)$ in the figures and shown superimposed. In general, when there are no unstable modes, thetwoplots converge to different values or oscillate independently and indefinitely in time, but whenever a mode with exponential growth is picked up by the code, they always converge coincidently to the same positive value.

Finally, fig.2(c) shows the radial profiles of the four perturbed pararneters B_{r1}, $B_{\Theta 1}$, V_{r1} and $V_{\Theta 1}$, each one normalized to their maximum values in the interval 0 - R_w, at any time in the exponential growth regime. To check the real nature of this mode, one has to look at the modification of the profiles of B_{r1} and V_{r1} with increasing value of S [4]. If, with an increase in S, the profile of B_{r1} near the wall depresses towards the axis (eventually crossing it) and the point where V_{r1} crosses the axis is displaced towards the wall (or alternatively maintains the same sign), then we have a typical case of a kink- dominated mode; otherwise, if the form of B_{r1} does not change significantly and the point where V_{r1} crosses the axis moves towards the singular surface, then we have a tearing-dominated mode. This is done for various values of q_a (representative of the whole interval of q_a for unstable modes) where S was raised to 5000. The corresponding plots for the typical value q_a = 2.4 are shown in fig. 3, where one can see that the functional form of B_{r1} has not been altered whereas the point where V_{r1} crosses the axis has been displaced towards the singular surface (marked with an arrow in this figure), indicating therefore that for a typical value of q_a where an unstable mode is present, this is essentially a tearing-dominated one.

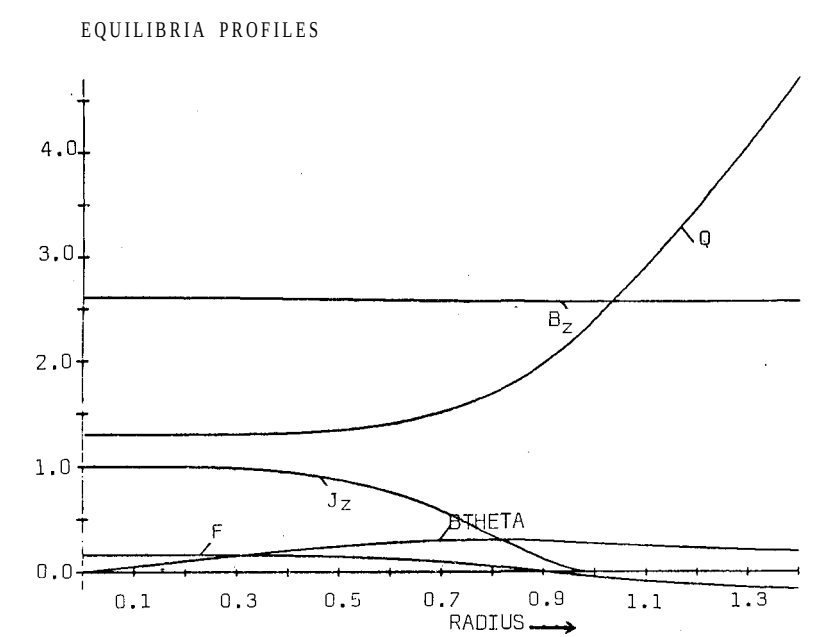

Fig. 2(a)

$B_{zo} = 2.60718$, $B_{za} = 2.56000$, $B_{ta} = 0.26702$, $R_s = 0.90728$, $F_o = 0.15695$, $Q_o = 1.30359$.

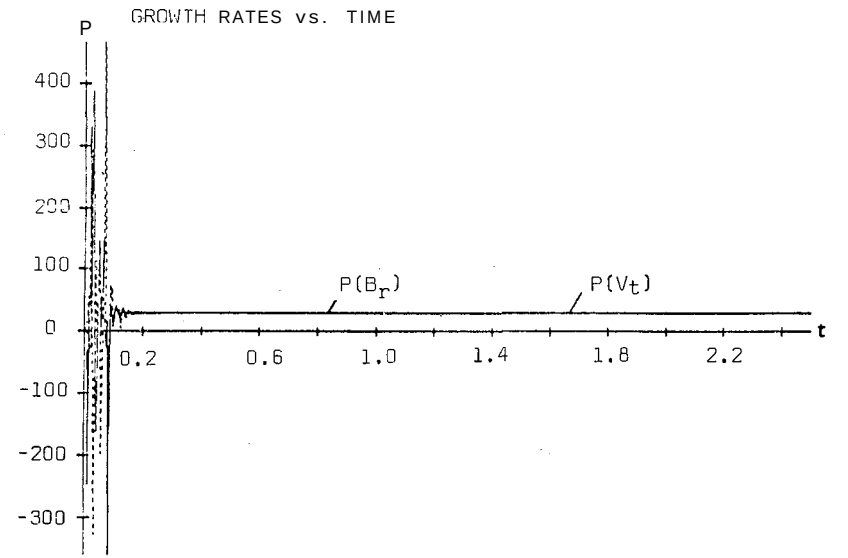

Fig. 2(b)

$Q_a = 2.400000$, $K_z = 0.25000$, S = 0.10000E 04, $P(B_r)$ = 0.2897BE 02, $P(V_t)$ = 0.2897BE 02.

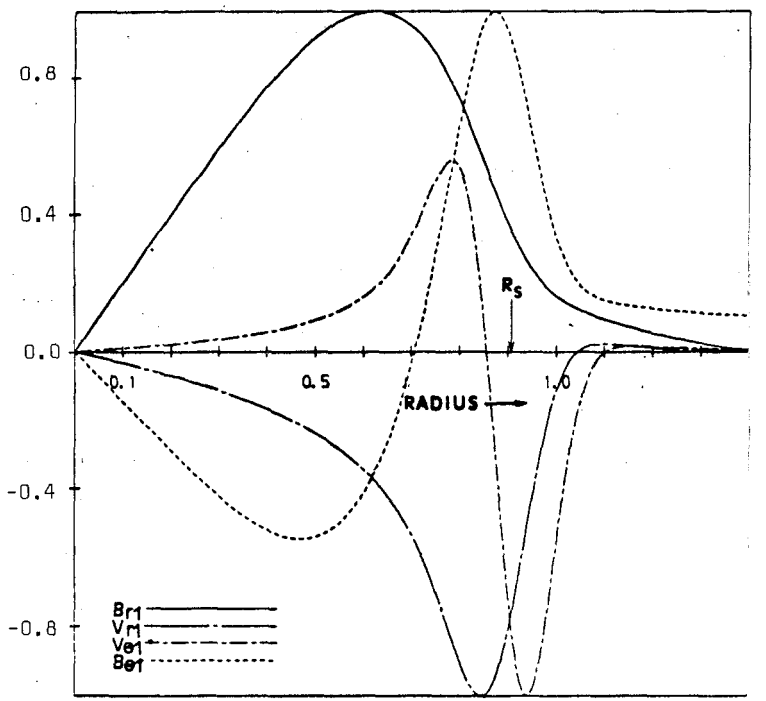

Fig. 2(c)

Fig.2 - (a) Equilibrium profiles for q_a = 2.4; (b) The normalized growth rate P versus normalized time; (c) Profiles of the normalized perturbed variables for the mode m=2, n=l and S=1000 along the normalized radius.

The same procedure has been followed with respect to the analysis of the nature of the unstable modes for the m=3, n=2 mode and the same conclusion has been reached, viz., all the modes represented in fig. 1 (curve m=3) are tearing modes. For this mode we present just representative case, viz., q_a = 1.8 and S = 1000, and q_a = 1.8 and S = 5000, shown in figs.4(a) and 4(b) respectively, where one can see that the point where V_{r1} crosses the axis has been displaced towards the resonant surface when S was raised to 5000. The remaining entry data are the same

a

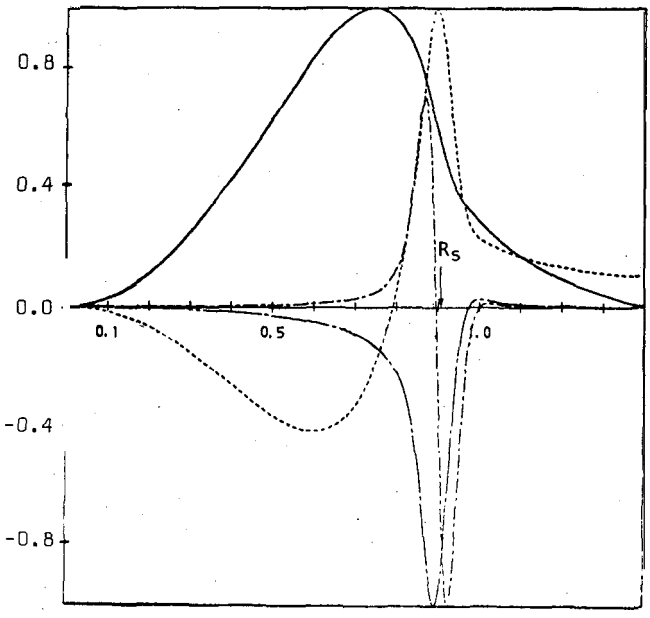

Fig.3 - As for fig.(c), except S = 5000.

as the ones used to run the cases in fiq. 1. One property of the m = 3 modes is that the perturbed profiles are more concentrated within the resistive layerascomparedwith thoçe from the m = 2 modes. This is because for. small r, $B_{r1} \sim r^{m-1}$ and for large r, $B_{r1} \sim 1/r^{m+1}$.

To close this section, we have plotted the growth rate Pagainst S for the m = 2 and m = 3 modes with q_a = 2.4 and q_a = 1.8 respectively (values of q_a for the maximum growth of the modes at S = 1000), and exhibited in fig. 5. As one can see from the figure the curves present a linear behaviour above S - 3000. If one describes this behaviour by the formula $P \propto S^K$, the value of K in the linear region (in the Log × × Log space) is 0.76 for the m = 2 and 0.756 for the m = 3 mode, well above the value of 0.4 presented by the sheet pinch[13] where the growth rate was found to obey the law $P \propto S^{2/5}$, but only a fraction greater than the one found with the peaked mode1[9], viz., K = 0.74.

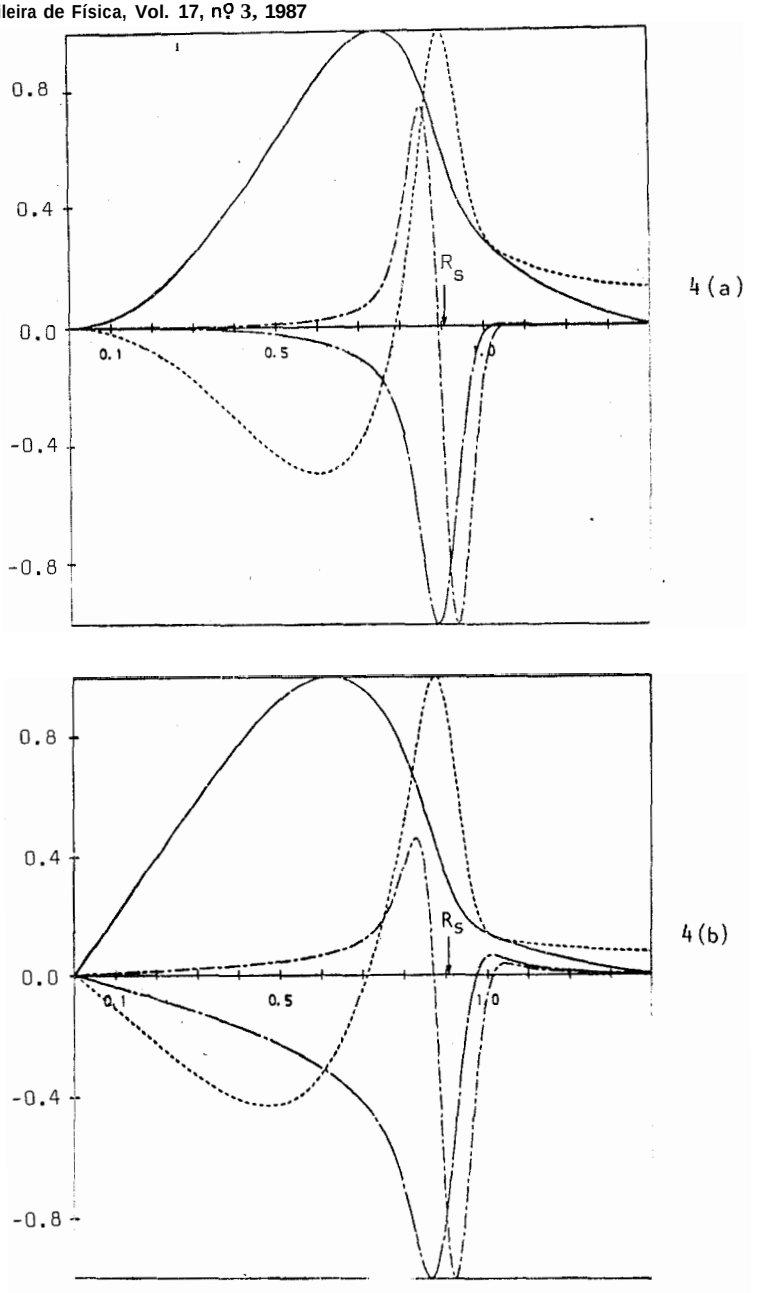

Fig.4 - (a), (b) Profiles of the perturbed variables for the m=3, n=2 mode with q_a=1.8 and (a) S = 1000 and (b) S = 5000.

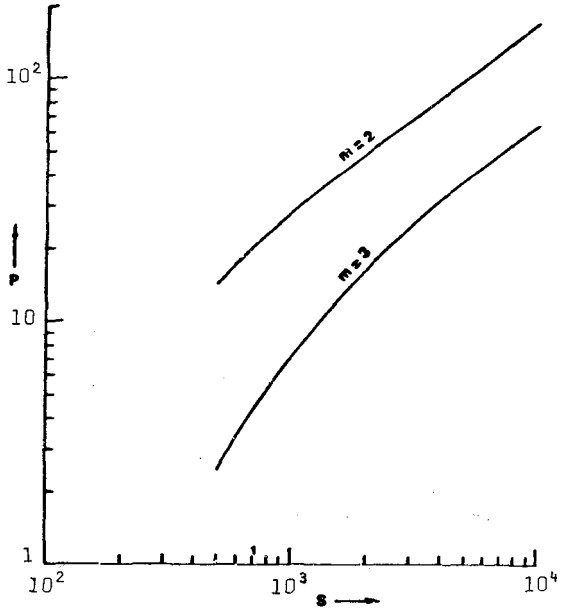

Fig. 5 - Growth rates P versus S for the modes m=2, n=1 with $q_a = 2.4$ and $m = 3$, $n = 2$ with $q_a = 1.8$.

(b). Numerical results with the modified Culharn Model

We now investigate how the growth rates of the unstable rnodes found previously are modified when a flat dip is imposed on the (otherwise smooth) current density profile. A provision for such a distorted current profile is already built in the code and consists of superimposing a gaussian function on a given smooth poloidal rnagnetic field profile $B_{\Theta_0}(r)$, viz., $B_{\Theta_0}(r) + S_1 \exp[-S_2(r-RR_1)^2]$, and the $J_{z_0}(r)$ current density is now adjusted according to formula (19). From B_{Θ_0} and J_{z_0} the code calculates B_{z0} using formula (22), and subsequentiy J_{Θ_0} using formula (27). The parameters $S_1(<0)$, $S_2(>0)$ and RR_1 control the height, the width and the position of the dip respectively. Fig. 6 shows a plot of the growth rate profile in q_a space in this new equilibrium (continuous line) and the corresponding old equilibrium case (see §(a)) (dashed lines) for comparison as well as a plot of the singular surface position x_s. The entry data for these new cases were as listed: N = 2, $M = 4$, $m = 2$, $k_z = -0.25$, $S = 1000$, $\tilde{R}_W = 1.4$, $\tilde{R}_0 = 4.$, $(S_1, S_2, RR_1) =$

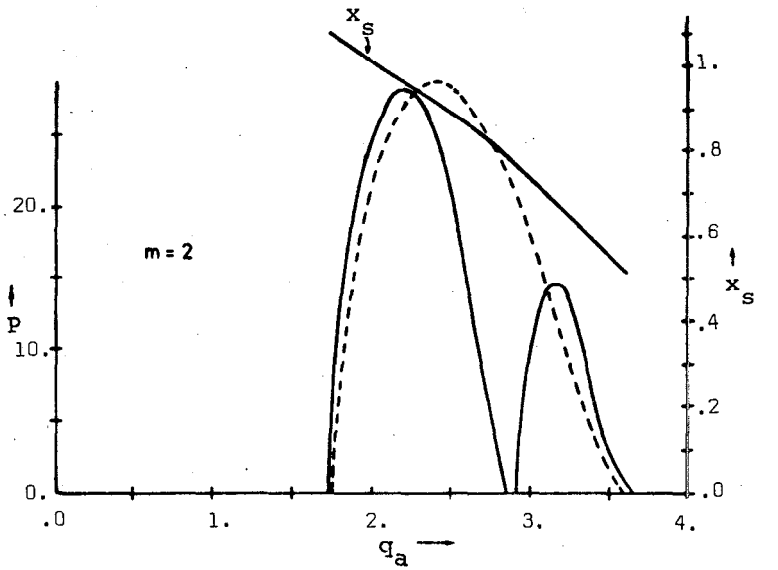

Fig.6 - As for fig.1 (m=2) with the addition of (Si, S_2, RR_1) = (-0.013, 75., 0.7). The curve in broken lines represents the standard curve for the m=2 mode shown in fig.1.

= (-0.013, 75, 0.7) (parameters for the plateau-like distortion), with $0 \leq q_a \leq 4.0$.

One can see from this figure that the same comment as in §(a) applies for x_s and most of the unstable modes appear in the same interval of q_a as in the old equilibrium but now a significant change takes place in the mid-interval: a small interval in q_a (a stability window) appears where no unstable modes exist. This window encompasses the interval $2.83 \leq q_a \leq 2.92$. The split of the standard curve P vs q_a of the old model into two branches however does not alter the maximum growth significantly nor its position in q_a space, this being 28.4 at q_a = 2.2 for one of the branches. The lower maximum on the other branch presents a value of 14.9 at q_a = 3.15, and its corresponding equilibrium perturbed profiles are shown in figs. 7(a),(b). These profiles look very much the same as those found in the standard case, presenting the same

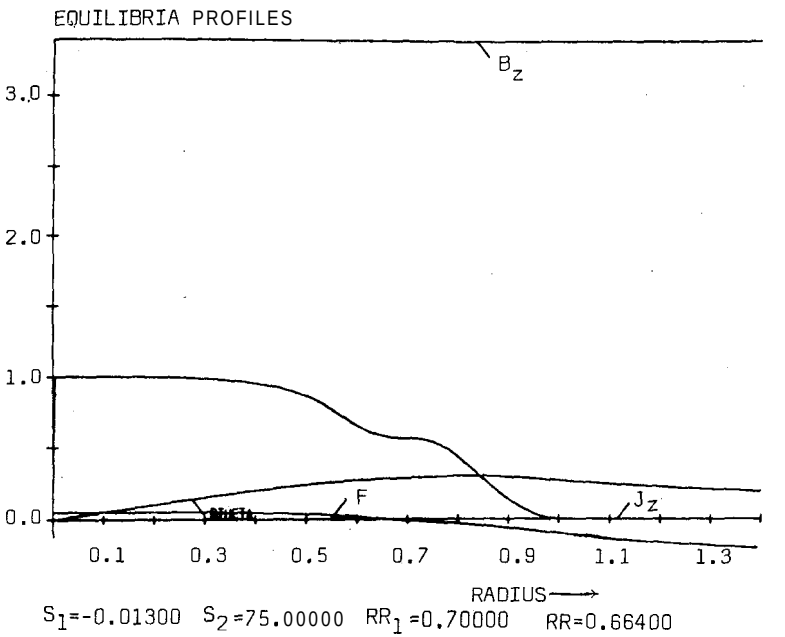

7(a)

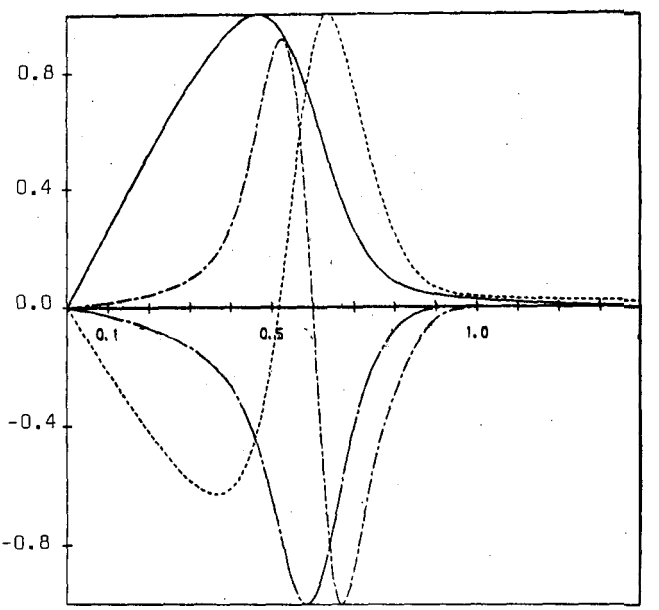

7(b)

Fig.7 - (a) Equilibrium and (b) perturbed profiles for the m=2 mode with q_a = 2.2.

tearing mode characteristics. The split of the curve P vs q_a into two branches therefore has not affected the nature of the modes.

Fig. 8 presents a very similar result for the m = 3, n = 2 mode, exçept that the split branch on the left has its maximum significantly higher than the standard curve, raising to a value 12.7 at q_a = 1.7, and the stability window between the branches has broadened to $2.06 \leq q_a \$2.31$; the second branch has a maximum 4.58 at q_a = 2.43, the smallest and the biggest value of q_a for instability having not been altered significantly from the standard curve, and now being q_{amin}=1.47 and q_{amax}=2.68.

Figs. 9(a) and (b) exhibit the equilibrium and perturbed profiles for the case q_a = 2.43.

An inspection of the plots depicted in figs. 6 and 8 shows that it is possible to inhibit and partially suppress a given mode (either m = 2 or m = 3). For the cases under study there is no overlapping of the stability windows in the parametric space q_a, as one can see by inspection of the two figures, but if one plays with the three par-

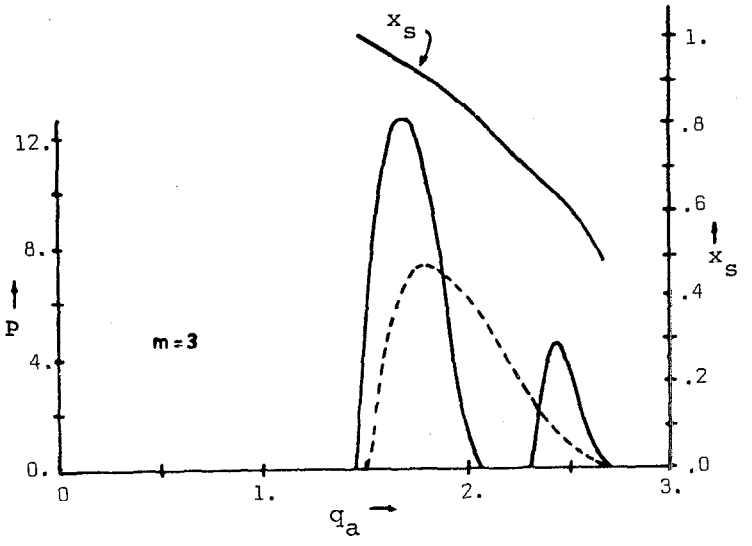

Fig. 8 - As for fig. 6 except m = 3, n = 2.

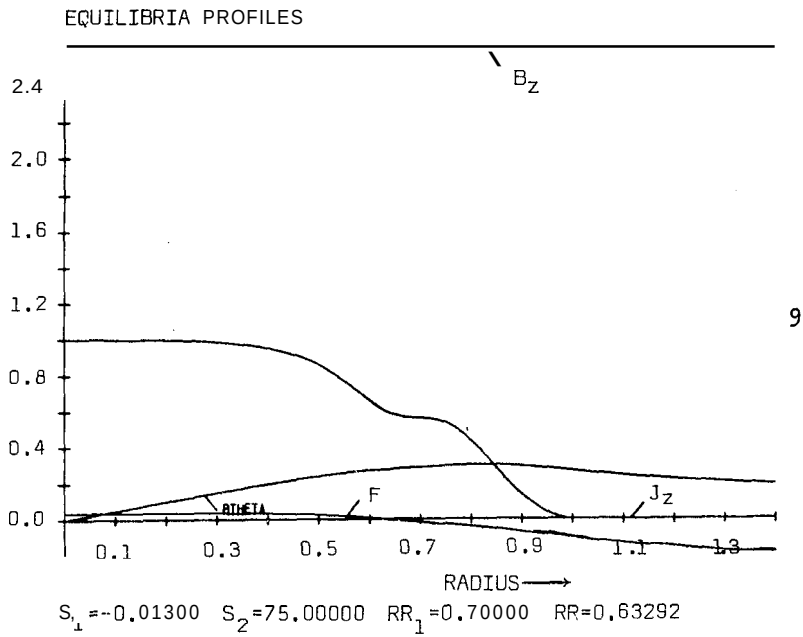

9(a)

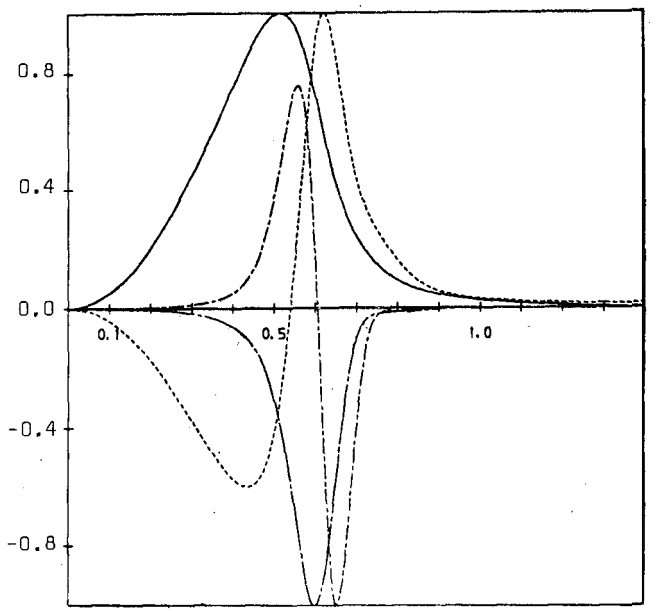

9(b)

Fig.9 - (a) Equilibrium and (b) perturbation profiles for the mode m = 3, n = 2 with q_a = 2.43.

ameters which control the shape and the position of the dip on the current profile the overlapping can be made to occur, henceforth avoiding the occurrence of both modes simultaneously by operating with q_a in this common window. Now, although the stability window in q_a for the m=2 mode encompasses values of q_a for which no m=3, n=2 mode is present (compare results which led to figs. 6 and 8) it would be of more interest to know whether such windows can be found in an other parametric space for any fixed value of q_a and whether such windows present overlapping. To verify whether this is feasible we have fixed the value of q_a at 2.2 for the m=2, n=1 mode and q_a = 1.7 for the m=3, n=2 mode (the values which correspond to the maximum growth for each mode), and varied the parameter RR_1 which controls the position of the dip. Note that each one of these values of q_a falls (incidentally) on the other ones stability window. Note also that by choosing these particular values of q_a, we would actually be looking for windows in RR_1 parameter space which might be valid for any other values of q_a (in particular, a value of q_a common to both modes).

The parameter RR_1 was made to assume values in the interval $0 \leq RR_1 \leq 1.4$. The other relevant parameters are listed as follows:

For the m = 2 mode, k_z = -0.25 (or n = 1), S = 1000, $\tilde{R}_W$ = 1.4, (S_1, S_2) = (-0.013, 75) (controls the form of the dip), $\tilde{R}_0$ = 4.; and the same as above for the m = 3 mode except k_z = -0.50 (or n = 2). The results are illustrated in fig. (10) with plots of growth rates versus

for both modes, where it is shown that the second maximums have raised above the first maximums (corresponding to the first maximums in fig. 6 and 8 for m = 2 and 3 respectively, where RR_1 was fixed at 0.7) with values 36.8 and 21.0 for the m = 2 and 3 modes respectively, both at q_a = 1.0. The growth rate for the m = 2 mode reaches the first minimum at q_a = 0.84 with the value 11.3. Now, only the mode m = 3 has presented a stability window in RR_1 space, viz., $0.80 \leq RR_1 \leq 0.91$, although we have taken the most favourable value of q_a to find an m=2 mode (at the maximum in fig. 6). It could be that by broadening the dip on the current profile and choosing other values for q_a such a window would also have appeared for the m = 2 mode. This result suggests that one should look for a two-dimensional stability window in (q_a, RR_1)

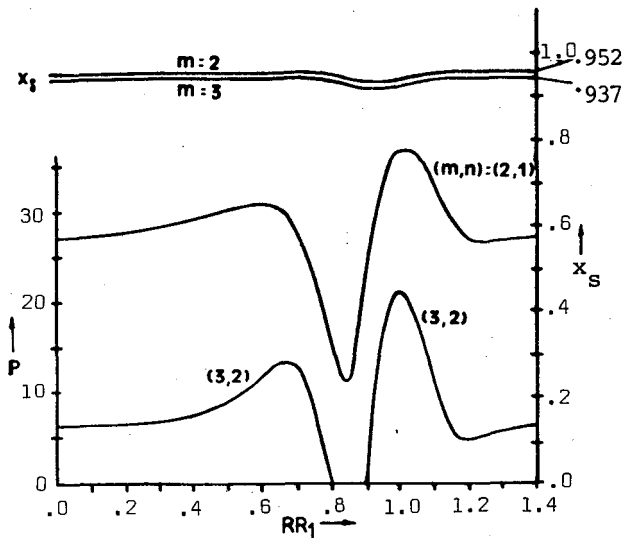

Fig.10 - Growth rate P versus RR_1, the position of the dip on the longitudinal current density profile for the $m = 2$, $n = 1$, tearing mode with $q_a = 2.2$ and $m = 3$, $n = 2$ tearing mde with $q_a = 1.7$. The position of the singular surfaces x_s for both modes are also plotted against RR_1.

space or even a three-dimensional one if S_2, which controls the width of the dip, were included.

Figures 11(a) - 13(b) illustrates three typical cases found with q_a taken from three distinct regions of the upper curve in fig.10 for the $m = 2$ mde and $RR_1 = 0.74$, 0.94 and 1.2. Fig. 11(a) shows a plateau-like distortion on the J profile produced with $RR_1 = 0.74$ and fig. 11(b) the corresponding perturbed parameters profiles, where one can see that their general forms are similar to those found on the left branch of fig. 6. This type of distortion is the one which most inhibits the growth of instabilities and frequently sought in practice. We note that the distortions on J shown in fig. 11(a) were such as to leave the original current channel radius unaltered (at $x = 1$). By further displacing the dip towards the right in 'fig. 10 it will come to a point where the growth rate begins to increase as a result of a broader current channel; this is exemplified with the case presented in figs.12(a)

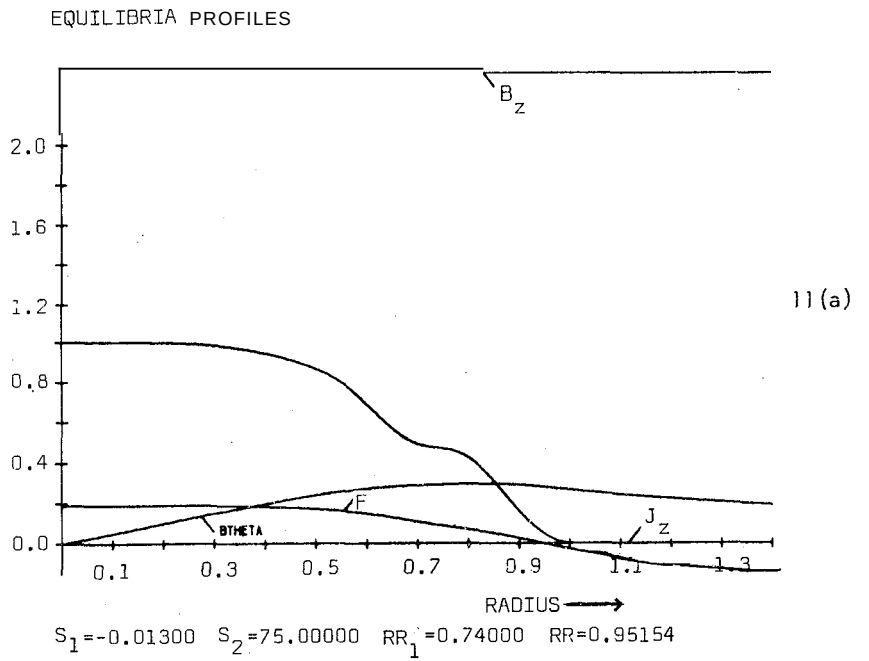

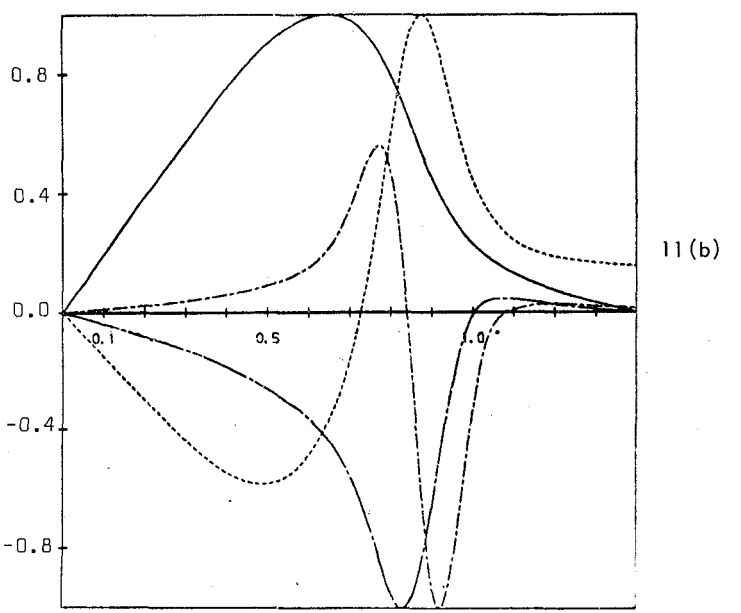

Fig. 11 - (a) Equilibrium and (b) perturbed parameters profiles for the $m = 2$, $n = 1$ mode with $RR_1 = 0.74$.

and 12(b) which is also a representative of cases where the dip falls just below the original current channel radius, the second maximum in fig. 10. Further to the right, the current profiles begin to develop a dip below the axis (representing an inverse current) and a lump above it. On the descending part of the curve in fig. 10, the dip is bigger than the lump and their contribution to the total current is negative, i.e., the *effective* current channel has been contracted thereby producing modes with lower growth. An example of this case is illustrated in figs. 13(a) and 13(b). Still on the descending part from some position of the dip to the next, however, its size decreases and the size of the lump increases until both contributions to the total current sum up to nil; this is what happens for the part of the curve on the extreme right in fig. 10. In the second and third cases presented above, the perturbed profiles look much the same as those found on the right of fig. 6.

The whole analysis for the $m = 2$ mode, presented before would follow similar lines for the $m = 3$ modes except that the lower plot in fig. 10 is interrupted by tke stability window, a small interval in the RR_1 axis, as mentioned before, and that the tearing mode character is still stronyer for the $m = 3$, $n = 2$ modes where one can see that the profiles are more concentrated within the resistive layer. Just one $m = 3$, $n = 2$ case is illustrated in figs. 14(a) and 14(b) corresponding to the value $RR_1 \approx 0.74$, showing that, apart from the slightly wave-like structure which develops inside the current channel radius, the perturbed profiles look very similar to the ones obtained with a smooth current density profile (see fiy. (3)).

4. DISCUSSION OF RESULTS AND CONCLUSION

An inspection of fiy. 10 indicates that the lowest vaiues of the growth rate are found when the position of the dip is close to and inside the singular surface. It is this fact that is commonly exploited at present in the experiments set up to inhibit instabilities by profile control in tokamaks, and whose main purpose is to delay or even suppress the disruptive process. The dip in the plasma current density

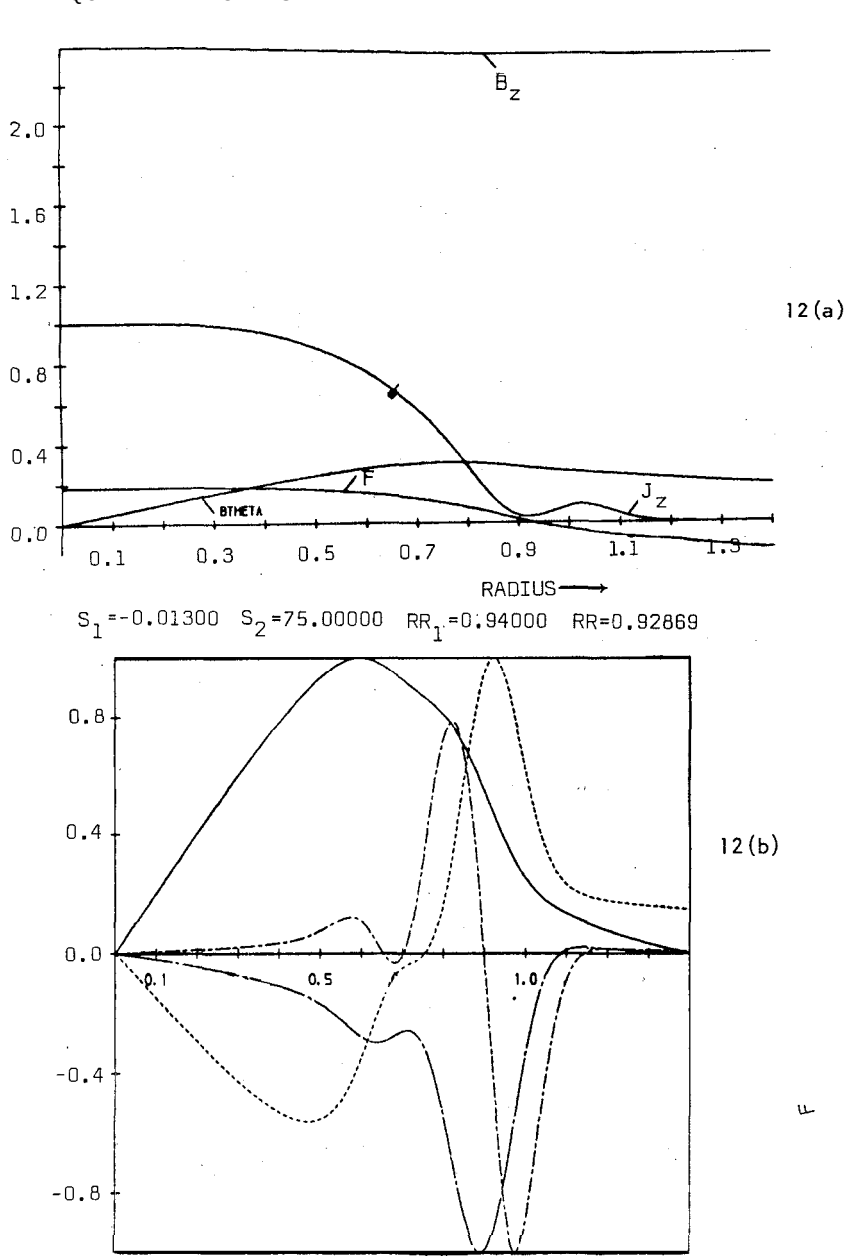

*Fig.*12 - ***(a)***, (b) - As *for fig.*11, *except* $RR_1 = 0.94$.

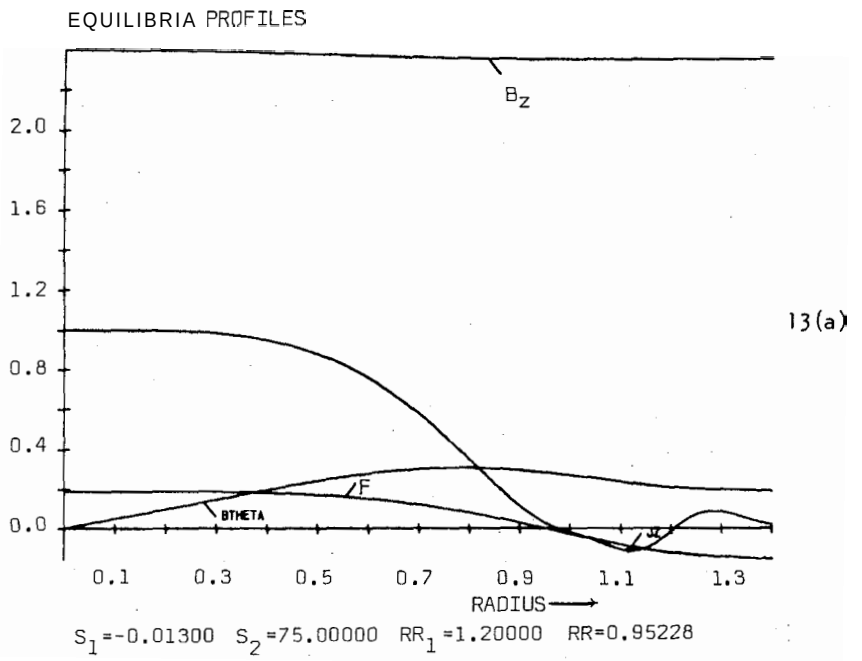

13(a)

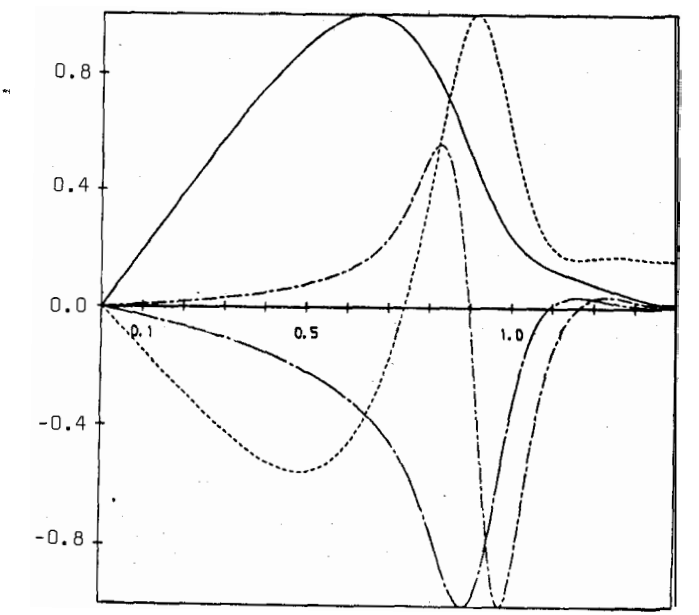

13(b)

Fig.13 - (a), (b) - As for fig.11, except RR_1 = 1.2.

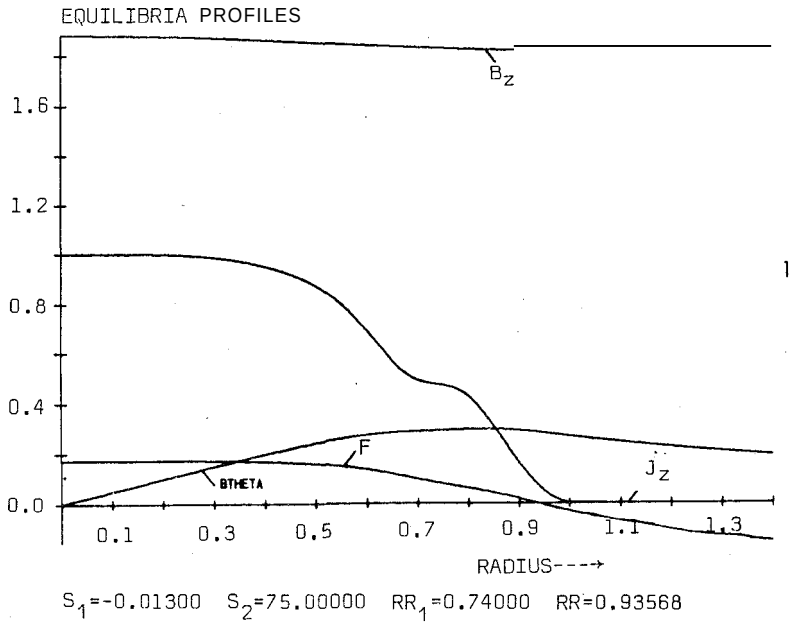

14(a)

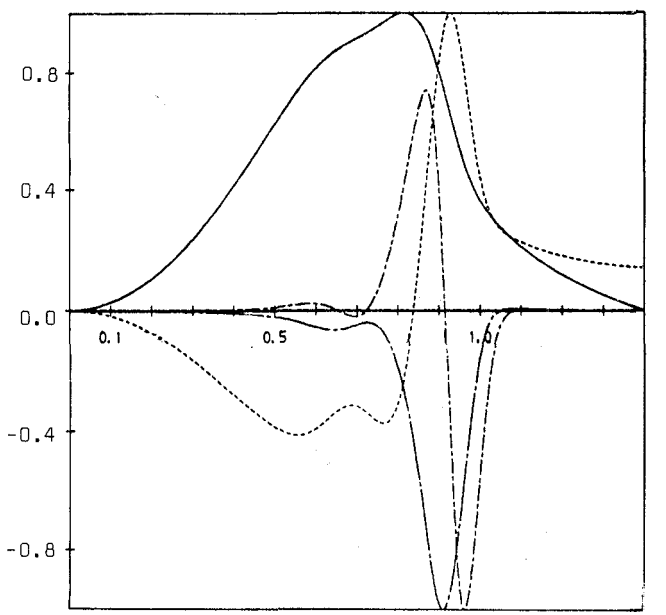

14(b)

Fig.14 - (a), (b) - As for fig.11, **except** m=3, n=2.

profile can be produced by using electron cyclotron waves for (locally) heating the plasma or driving a current in opposite direction at some position inside the singular surface.

In this work, we have shown that although an overlapping of stability windows in q_a space could not be found for the resistive tearing m = 2, n = 1 and m = 3, n = 2 modes, one can operate with q_a in the window for the m = 2, n = 1 mode with no occurrence of the m = 3, n = 2 modes, as one can see by noting that the window in the mid-interval of q_a for stability of the m = 2, n = 1 mode (fig. 6) falls on the right of the interval of q_a for the existence of the m = 3, n = 2 mode (fig. 8). The necessity of operating with lówer values of q_a in the various experimental conditions, however, makes it desirable to find windows of stability in another parameter space, viz., the position RR_1 of the dip of the distorted current profile. The corresponding search however led to the finding of a stability window in the parameter space RR_1 only for the m = 3, n = 2 mode although the growth of the m = 2, n = 1 mode has been greatly inhibited (but not suppressed) in that interval of RR_1 (fig. 10).

D.C. Robinson et al[4] succeeded in finding the equilibrium configuration which led to the complete stabilization of both modes simultaneously, but the so-called Tearing Mode Stable Model used presents two dips on the current density profile, conveniently positioned inside the q = 2 and q = 3/2 singular surfaces. In our search for stability windows in RR_1 space we were more interested in current profiles presenting just one dip because, for obvious reasons, the corresponding equilibrium configuration would be easier to analyse theoretically and to achieve experimentally. Now, the minirnum at the trough of the m = 2 curve in fig. 10 is not low enough, perhaps due to the particular values of q_a, which were chosen amongst the most favourable to find both modes (each of these values leads to the respective maximums depicted in figs. 6 and 8). With some adjustement of these values, one might possibly reduce the growth of the unstable m = 2 mode to acceptable levels, say below or of the order of the field diffusion rate ($\gamma \approx 1/\tau_R$ and therefore P = 1). This it at present under consideration by the author together

with the case which uses a common q_a (a common total current) for different positions (RR_1) of the dip.

The results presented here are of course not complete nor rigorous for establishing stability windows, for we have not controlled the shape of the dip (through S_1 and S_2) nor tried other values of q_a in looking at windows in RR_1 space. A more rigorous treatment of this problem would involve the use of a non-linear resistive code where the saturation of the modes could also be examined as well. It nevertheless reasserts the method of instability control by plasma current shaping and paves the way for establishing the set of parameters needed in experimental set ups to realize a discharge with control of the most dangerous instabilities in pinches and tokamaks.

The author thanks Culham Laboratory, UK, for the use of its facilities and Dr. D.C.Robinson for the suggestion of this work and helpful discussions, as well as Mr. Paul Haynes for his invaluable advice on the existing computing system at Culham.

The author was partially supported by Conselho Nacional de Desenvolvimento Científico e Tecnólogico (CNPq), Brasil.

REFERENCES

1. M.F.Turner, J.A.Wesson, Nuclear Fusion, 22, 8, 1069 (1982).
2. K.Toi, *et al*, Nuclear Fusion, 19, 1643 (1979).
3. D.F.H.Start, Proc. 3rd Joint Varenna-Grenoble Int. Symp. on Heating in Toroidal Plasmas, Grenoble, CEC *3*, 849 (1982).
4. D.C. Robinson, *et al*, Culham Laboratory Report CLM-P710.
5. A.H. Glasser, *et al*, Phys. Rev. Letters, 38, 234 (1977).
6. J. Killeen, in *Physics of Hot Plasmas*, Ed.Plenum Press, N.Y., (1970).
7. J.A. Dibiase, J. Killeen, Journal of Computational Physics, 24,158 (1977).
8. H.P. Furth, *et al*, Physics of Fluids, 16, 1054 (1973).
9. J.E. Crow, *et al*, Proc. 6th European Conference on Controlled Fusion and Plasma Physics, Moscow (1973).
10. A.H. Glasser, *et al*, Physics of Fluids, 18, 875 (1975) and 19, 596 (1976).

11. V.D. Shafranov, Soviet Physics-Technical Physics, 15,2,175 (1970).
12. H.P. Furth, et al, The Physics of Fluids, 6, 4, 459 (1963).

Resumo

Um código computacional baseado num esquema implícito de diferenças finitas foi empregado para resolver um conjunto de equações diferenciais parciais (dependentes radial e temporalmente) para as variáveis perturbadas que descrevem a instabilidade magnetohidrodinâmica (MHD) resistiva em pinches e tokamaks, a fim de estabelecer as condições para o aparecimento de janelas de estabilidade em alguns dos espaços paramétricos (parâmetros livres) usados. Mostrou-se que é possível inibir ou mesmo suprimir os modos *tearing* m=2, n=l e m=3, n=2 por deformação do perfil da densidade de corrente longitudinal do plasma na forma de uma pequena e localizada distorção sobre um perfil liso previamente escolhido para a configuração de equilíbrio. As janelas correspondentes aparecem no espaço paramétrico dos q_a, o fator de segurança na posição do canal de corrente, para uma posição fixa da distorção, assim como no espaço paramétrico das RR_1, a posição radial da distorçáo, para um valor fixo de q_a; em ambos os casos, a distorção é localizada próxima e dentro da superfície singular.